Received: 4 November 2025 | Revised: 4 February 2026 | Accepted: 5 February 2026

DOI: 10.1111/jmi.70068

Journal of Microscopy RMS

METHODS AND PROTOCOLS

A detailed protocol for open and low-cost six-plex immunofluorescence (Flex-6 mIHF) with a proof-of-concept study on breast cancer tissue

Julia A. M. Riggi[1,2] | **Aurélie Daumerie**[3] | **Naïma Benhaddi**[1] | **Martine Berlière**[4,5] | **Christine Galant**[1,2] | **Alicia González-Antelo**[1] | **Frank Aboubakar Nana**[6,7] | **Mieke R. Van Bockstal**[1,2] | **Caroline Bouzin**[3]

[1]Department of Pathology, Cliniques universitaires Saint-Luc, Brussels, Belgium

[2]IREC, Pôle MORF, UCLouvain, Brussels, Belgium

[3]IREC, Imaging Platform (2IP – RRID:SCR_023378), UCLouvain, Brussels, Belgium

[4]Breast Clinic IRAII, Cliniques universitaires Saint-Luc, Brussels, Belgium

[5]IREC, Gynecology Research Unit, UCLouvain, Brussels, Belgium

[6]Department of Pulmonology, Cliniques universitaires Saint-Luc, Brussels, Belgium

[7]de Duve Institute, TILS, UCLouvain, Brussels, Belgium

Correspondence: Caroline Bouzin (caroline.bouzin@uclouvain.be)

Funding information
Fund for Scientific Research-F.N.R.S, Grant/Award Numbers: 40033175, 35287957; Foundation Against Cancer, Grant/Award Number: 2025–048

Abstract

Multiplex immunohistofluorescence (mIHF) allows to investigate protein (co)-localisation in the tumour microenvironment, which can facilitate research on carcinogenesis. Most available technologies for multiplex staining are expensive and immutable. We aim to demonstrate the feasibility and the flexibility of a low-cost mIHF protocol through the illustrated fine-tuning of two six-plex panels on human breast cancer samples. We detail a workflow combining two fluorescence amplification steps – (1) a peroxidase-labelled polymer conjugated to secondary antibodies and (2) tyramide signal amplification technology – to overcome the high autofluorescence of FFPE sections. The optimised slide scanner configuration enables single-run acquisition of up to six markers plus a nuclear dye from one tissue section. The resulting native scans can be directly used for analysis without the need for extensive or complex image processing. As a proof of concept, this protocol was applied on breast tissue samples from 19 patients diagnosed with ductal carcinoma in situ (DCIS), of various size, age and fat content. Two six-plex panels highlighted proteins expressed in tumours cells, extracellular matrix, and lymphocytes. The 12 proteins were first individually validated by immunohistochemistry, subsequently by immunohistofluorescence and finally combined in two six-plex panels. Only one sample could not be interpreted. Some samples displayed tissue detachment, cold zones or heterogeneous immunoreactivity, independently of the fat content, surgical procedure or specimen age. Here, we propose an open, flexible and cost-effective six-plex protocol (Flex-6 mIHF) and a validation workflow. We demonstrated its feasibility on challenging tissue containing fat such as breast cancer tissues.

KEYWORDS

breast cancer, immunohistochemistry, low-cost, multiplex immunofluorescence, protocol, tumour microenvironment

1 | INTRODUCTION

Breast cancer treatment has become increasingly precise, evolving from non-selective chemotherapy to therapies targeting specific receptors on cancer cells or immune cells. Understanding the complexity of the tumour microenvironment and the immune response during carcinogenesis is key for the development of future therapies.

Colocalisation studies of proteins become increasingly important to facilitate our understanding of this complex interplay. Conventional bright-field immunohistochemistry (IHC) is falling short to support these increasing requests, because this technique only permits staining of a single marker per tissue section.[1]

To visualise several markers in a single tissue section, immunofluorescence is used rather than chromogenic IHC to facilitate colour deconvolution. Multiplex immunohistofluorescence (mIHF) offers diverse advantages. Firstly, mIHF enables to investigate protein expression in tissue samples of limited size. It also allows the assessment of spatial cellular distribution of biomarkers to characterise the tumour microenvironment and its interaction with neoplastic cells.[2] mIHF has been shown to be of utmost importance to decipher the immune response against cancer, showing differences in protein expression between pre- and post-treatment tissue samples.[1,3]

Fluorescent co-staining of several markers on a single histological slide can be achieved in different ways.[1,4] For 'simple' co-staining of three or four markers, indirect immunofluorescence is the most common approach This technique applies primary antibodies either directly coupled to fluorophores or unconjugated from different host species or conjugated to DNA barcodes and corresponding secondary antibodies/probes coupled to a fluorescent dye. The main advantage of this method is its scalability. After imaging of the 3–4 markers, antibodies can be stripped or the fluorochrome can be inactivated or cleaved, and new cycles of staining/imaging can be performed on the same tissue section. High-plex (up to 118-plex) staining protocols have been generated this way.[5–7] However, the high autofluorescence of formalin-fixed paraffin-embedded (FFPE) sections often masks the fluorescence signal related to antibodies, rendering them insufficiently bright. To overcome this issue, one solution is to process the generated image for background subtraction, which is time consuming and therefore inconvenient. Images generated after each staining cycle also need to be perfectly aligned, which requires quite high computational power and plenty of time.

A way to improve the signal-to-noise ratio is to use the Tyramide Signal Amplification (TSA) technology in which fluorescent dyes are more abundant and covalently linked to the tissue and not to the antibodies. This amplification method generates much brighter signals than the strong autofluorescence of FFPE samples. Sequential single staining can be performed with antibodies being stripped after each staining cycle. This antibody removal allows the use of subsequent primary antibodies raised in the same species. The downside of this method is its limited scalability. Since dyes are covalently linked to the tissue, they cannot be detached/stripped. The number of dyes per section is then limited to the number of dyes detectable in the visible spectrum with a minimal spectral overlap. This has been raised to 8 colours by Akoya Biosciences (Massachusetts, USA) (PhenoImager HT; formerly Phenoptics-Vectra Polaris) but requires time and computer-intensive background subtraction and spectral unmixing post-processing.

Recently, Cell Signaling Technology (Massachusetts, USA) proposed an alternative way of signal amplification, designated SignalStar™, based on primary antibodies associated with DNA barcodes revealed by branched DNA fluorescent probes. Lunaphore also proposed an enhancement of detection of secondary antibodies bound to primary antibodies by utilising linker molecules (SPYRE amplification). These technologies are nevertheless limited by their high cost and/or the restricted availability of primary antibodies.

High-plex can also be achieved with a mass spectrometry readout by using direct ionisation (Imaging Mass Spectrometry) or antibodies conjugated to metal reporters (Multiplexed Ion Beam Imaging). These technologies are very expensive and technically challenging, as they comprise matrix application on samples, instrumentation complexity, and provide large data size.

Here, we focus on low-plex technologies and detail a more open and cost-effective workflow of mIHF. We aimed to illustrate its feasibility and flexibility through the fine-tuning of two six-plex panels on human breast cancer FFPE samples, including both biopsies and surgical resection specimens. Additionally, we highlight how the Flex-6 mIHF workflow positions among the major commercial technologies.

2 | METHODS

2.1 | Chromogenic immunohistochemistry – antibody validation

2.1.1 | Antibody selection

The selection of each primary antibody and its validation is crucial. To guide this selection, the following guidelines should be considered:

- Species compatibility

The antibody should recognise the target species. The antibody should be raised in another species than the target species. Commercial products (mouse-on-mouse, etc.) can limit the detection of native immunoglobulins present in the section but most of the time will not completely prevent their detection, leading to nonspecific staining.

-Technical compatibility

For FFPE sections, antibodies should be recommended for IHC-P. When 'IF' is mentioned in the datasheet of an antibody, this is usually related to immunofluorescence on cultured cells, not on FFPE sections.

- Clonality

When possible, favour monoclonal antibodies to achieve better batch-to-batch reproducibility. However, for proteins with limited expression or with a wide expression range (weak to strong staining intensity), polyclonal antibodies may prove their superiority.

- Provider selection

Commercial companies do not use identical methods for the purification and validation of primary antibodies. Therefore, the same clone from different providers will not always behave in the same way. NordiQC, a scientific organisation whose goal is to promote the quality of IHC, provides useful information to select the most appropriate antibodies for human samples.[8]

Some of these requirements can be found in the datasheets of the primary antibodies but this information needs to be cross-checked using different databases and, mainly, compared with published data.

2.1.2 | Slides preparation

All reagents and equipment used in the following protocol are described in Table S1.

1. Section the FFPE blocks at 4 µm. Thicker sections (sometimes needed for specific tissue types such as brain or striated muscle) can lead to tissue detachment from the slides and will result in difficulties with staining interpretation due to superimposed cells.
   NB: Avoid placing sections close to the slide borders, especially if using an autostainer.
2. Place the sections on Superfrost Plus slides (Menzel-Gläser, Braunschweig, Germany) and let them dry at 37°C for 24 h.
   NB: Using non-positively charged glass slides may lead to tissue detachment during heating steps
3. Store slides at room temperature (RT) in a dry environment, ideally placing desiccant bags in the storage box, for maximum 6 weeks.
4. The day before the immunostaining: place the slides at 37°C overnight until the next step, to improve section adhesion and to soften paraffin.

Dewaxing and rehydration – *Timing 30 min*

This step aims to completely rehydrate the tissue sections since IHC requires an aqueous environment.

5. Dewax the sections by immersing the slides into three successive baths of toluene. Leave the slides for 5 min in each bath after 10 upward and downward movements.
   NB: Incomplete paraffin removal will lead to inhomogeneous staining.
6. Rehydrate the sections in three successive baths of isopropanol. This solvent is used as it is miscible with both toluene and water. Leave the slides for 5 min in each bath after 10 upward and downward movements.
   ! Harmful substances: perform dewaxing and rehydrating under a fume hood.
   NB: Gently dab the slides on a paper towel between toluene and isopropanol to remove excess liquid, to avoid contamination of the isopropanol bath.
   NB: Change baths regularly.

Inactivation of endogenous peroxidases – *Timing 20 min*

This step avoids nonspecific detection of peroxidases that are naturally present in different cell types, such as erythrocytes and neutrophils.

7. Prepare a 3.5% H_2O_2 solution (20 mL of 35% H_2O_2 in 180 mL of isopropanol) and immerse the slides for 20 min.
8. Wash the slides in a bath of distilled water during 5 min.

Heat-induce epitope retrieval (HIER) – *Timing 30 min*

This step is necessary to reverse the chemical modifications of proteins mediated by formaldehyde and hence to make the antigen accessible to the antibody. It is required for most antigens. The choice of low or high pH is determined empirically.

9. Prepare low pH and/or high pH solutions as follows.
   → *Low pH*: add 25 mL of citrate buffer stock solution 10× concentrated (detailed in Table S2) and 675 µL of 20% Triton-X100 solution (diluted in distilled water) in 225 mL distilled water.
   → *High pH*: add 25 mL of Tris-EDTA buffer stock solution 10× concentrated (detailed in Table S2) and 675 µL of 20% Triton-X100 solution (diluted in distilled water) in 225 mL distilled water.
10. Immerse the slides into a microwave-proof container filled with the appropriate solution. Place the container in the microwave at 900 watts (or maximum

power) until boiling (approximately 4 min 30 s). Place the container subsequently at 90 watts during 15 min, and finally at 900 watts (or maximum power) until the solution is boiling again (approximately 1 min 30 s).
NB: If the slide holder is not entirely filled with slides, fill the empty positions with glass slides to even out the heat for all slides.
NB: For reproducibility purposes, always use two containers filled with slides in the microwave: if slides of interest are insufficient to fill two containers, complete with empty/ghost slides.

11. Wash the slides in a bath of distilled water during 5 min, and subsequently in Tris-buffered saline (TBS, detailed in Table S2) containing 0.1% Tween 20 (TBST, detailed in Table S2) during 2 min.

Blocking of antibody binding to non-specific sites – *Timing 30 min*

12. Place the slides flat in a humidified box.
13. Wipe the glass slides with a paper towel at a secure distance from the tissue section to remove excess liquid and to limit subsequent spreading of solutions and hence reduce the required reagent volume.
NB: Circling the tissue section with a hydrophobic pen is possible but is not recommended as the pen ink generates strong autofluorescence that can interfere with signal detection, even if it does not contact the tissue directly.
14. Cover the sections with TBST containing 5% bovine serum albumin (BSA, detailed in Table S2). Close the box and incubate for minimum 30 min at RT.
NB: During the entire staining procedure, never let the slides dry out as this can cause background staining. For large batches of slides, treat a limited number of slides at a time.

Primary antibody incubation – *Timing 1 h 10 min*

15. Dilute primary antibody to the desired concentration in TBST containing 1% BSA (detailed in Table S2).
NB: If using an autostainer, add glycerol to this solution to limit antibody sedimentation (see Table S2).
16. Drain the blocking solution from the slides and wipe the slides at a secured distance from the tissue section with a paper towel.
NB: Do not wash the slides between blocking and primary antibody.
17. Cover the sections with the antibody solution and incubate for 1 h at RT. Depending on the section size, use 50 to 150 µL.
NB: When testing an antibody, start by testing three concentrations of antibody: 1, 5 and 10 µg/ml.
NB: Some antibodies require an overnight incubation at 4°C. This is less suitable for multiplex staining and/or for automation.
NB: For a better preservation of antibodies at –20°C, it is recommended to add an equal volume of glycerol, if it is not already present (information provided in the datasheet of the primary antibody).
NB: Avoid antibody incubation at temperatures higher than 25°C to avoid non-specific staining and section drying.
NB: Check the absence of nonspecific binding of revelation reagents by incubating slides without the primary antibody (i.e. negative control).
NB: Isotype control antibodies only reveal Fc-mediated nonspecific binding and do not provide evidence of Fab-dependent antigen specificity.
18. Wash the slides in TBST at RT (dip it up and down 10 times and then leave to rest in an incubation bath for 2 min – repeat this 3 times).
19. Carefully wipe the slides with a paper towel at a secured distance from the tissue section to remove excess liquid.

Secondary antibody incubation – *Timing 50 min*

20. Cover the sections with the appropriate secondary antibody during 40 min. Depending on the section size, use 50 to 150 µL of the ready-to-use solution.
NB: Secondary antibody has to be specific of the species of the primary antibody.
NB: To subsequently transpose the protocol to mIHF-TSA, select secondary antibodies conjugated to polymers labelled with several peroxidases (e.g. Agilent EnVision+ systems, Agilent, Santa Clara, CA, USA).
NB: If polymer-conjugated HRP-antibodies are not available for a specific species, use an intermediate secondary antibody before using polymer-conjugated antibodies labelled with HRP (e.g. for a rat primary antibody, use an unconjugated rabbit anti-rat followed by polymer-conjugated anti-rabbit).
21. Wash the slides in a bath of TBST at RT (dip it up and down 10 times and then leave to rest in an incubation bath for 2 min – repeat this 3 times).
22. Carefully dab the slides on a paper towel to remove excess of washing solution.

Revelation – *Timing 20 min*

23. Add 3,3'-diaminobenzidine (DAB) solution on the slides and incubate during 5 min at RT.
! Harmful substance. Wear gloves.
24. Wash the slides in two baths of distilled water.
25. Add haematoxylin to the slides during 5 min at RT.

NB: The Dako haematoxylin ref S3301 (Agilent) has been selected for its very high nucleus/cytoplasmic staining ratio, which facilitates cell segmentation during image analysis.

26. Wash the slides in tap water during 4 min under low flow, then in distilled water during 30 s.
    NB: Distilled water will not allow nuclei to turn blue.
27. Air-dry slides for at least 20 min.
    NB: Drying under chemical hood accelerates drying.

Mounting – *Timing 25 min*

28. Immerse slides in two successive baths of xylene.
    ! Harmful substances. Carry out manipulations in a fume hood.
29. Mount slides with a Tissue-tek film coverslipper (Sakura Finetek Europe, Alphen aan den Rijn, The Netherlands) or, alternatively, manually using organic mounting medium and glass coverslips.
30. Dry slides under the fume hood during 20 min.

2.2 | Immunohistofluorescence – tyramide signal amplification

The TSA technology described here contains two amplification levels: (1) secondary antibodies linked to peroxidase-conjugated polymers (e.g. EnVision+/HRP systems, Agilent) and (2) tyramide substrates conjugated to fluorescent dyes. The combination of these two amplifications is needed to increase the fluorescence signal above the high autofluorescence of FFPE samples as shown in Figure S1.

The same protocol is used for chromogenic IHC and fluorescent IHF-TSA. The only difference between these two protocols is the peroxidase substrate (DAB for IHC and fluo-tyramides for IHF, illustrated in Figure S2), counterstaining and mounting steps. All the other reagents are same as the chromogenic IHC protocol. In our experience, there is no need to adjust antibody dilution between IHC-DAB and IHF-tyramide.

2.2.1 | Slides preparation to secondary antibodies

Proceed to **steps 1 to 22** of the chromogenic IHC protocol.

Revelation – *Timing 15 min*

23'. Dilute fluorochrome-conjugated tyramide to the desired concentration in borate buffer containing 0.003% H_2O_2 (detailed in Table S2).
    NB: Higher H_2O_2 concentration will inhibit peroxidase while lower concentration will not allow optimal peroxidase activity, both leading to staining of low intensity.
    NB: From a 35% H_2O_2 stock solution, prepare an intermediate solution 100× diluted (1 µL 35% H_2O_2 + 99 µL distilled water) which will be further diluted 100× (1 µL intermediate solution + 99 µL borate buffer).
    NB: Diluted solutions can be kept for a few days at 4°C.

24'. Add the tyramide solution to the sections and incubate for 10 min at RT.
    ! Harmful substances. Wear gloves.

25'. Wash slides in TBST at RT (dip it up and down 10 times and then leave to rest in an incubation bath for 2 min – repeat this 3 times).
    NB: CF754-tyramides generate high background which disappears after an additional HIER step.

Counterstaining – *Timing 10 min*

26'. Cover slides during 5 min at RT with a solution of 10 µg/mL of Hoechst 33342 diluted 1000× in distilled water from the stock solution (see Table S1).
    ! Harmful substance. Wear gloves.

27'. Wash the slides in TBST once and subsequently wash them 3 times in distilled water.

2.2.2 | Mounting

For fluorescence preservation, the use of a dedicated aqueous mounting medium is required. In our experience, the Dako fluorescence mounting medium prevents from bleaching for a large array of dyes, including dyes in the far-red spectrum.

28'. Place a glass coverslip on a paper towel.

29'. Pour a line of fluorescence mounting medium on one of the long edges of the coverslip.
    NB: Conserve the mounting medium vial upside down in the fridge to minimise bubbles.
    NB: Remove the first drop, which may contain bubbles.
    NB: Another way is to apply the mounting medium directly on the section.

30'. Place one slide at an angle on the border of the coverslip and lay it prudently on the section.

31'. Apply light pressure on the slide during 30 s. Avoid tissue damage by avoiding twisting movements.
    NB: If the mounting is incorrect, it is possible to start again after removing gently the coverslip by

bathing slides in distilled water until the coverslip spontaneous detaches.

32'. Clean the excess of mounting medium with a water-soaked towel.

33'. Circle the tissue with a black marker at a distance of 1 mm from the section on the back of the slides to prepare them for fluorescence scanning.
NB: Markers of another colour (blue, red, green) will create fluorescence background.

34'. Store the slides at 4°C in the dark until scanning. Avoid exposure to light.
NB: Tyramide-labelled slides show minimal photobleaching and maintain signal integrity over extended periods.

2.3 | Multiplex immunohistofluorescence

With the TSA technology, fluorescent dyes are covalently linked to the tissue (not to the antibodies). This allows to perform sequential staining with antibodies being stripped after each staining cycle and revealed with different dyes, to reach multiplex staining. Of note, antibody removal allows the use of subsequent primary antibodies raised in the same species.

2.3.1 | Cycling IHF – antibody stripping

Antibodies are stripped using a new HIER step.

Proceed to the IHF protocol. After **step 25'**, repeat protocol from **step 9 to 22** (HIER, blocking and antibodies) **and 23' to 25'** (tyramide) for each other primary antibodies of the multiplex.

NB: Antibody stripping is more efficient using a microwave rather than a water bath.

NB: IHC and mIHF can be automatised using autostainer devices equipped with heating components (e.g. Leica BOND, Leica Biosystems, Nussloch, Germany) to allow repeated HIER steps.

NB: The nuclear counterstaining is performed only once, after the last cycle of IHF.

2.3.2 | Multiplex panel design – selection of fluorescent dyes

The selection of the fluorescent dyes depends primarily on the configuration of the slide scanner (cfr Section 4).

Each antibody can be tested in combination with each dye but taking into consideration the following factors is usually sufficient to assign the dyes to the primary antibodies of a specific panel.

TABLE 1 Fluorescent dyes up to six-plex.

	CF430	CF488	CF555	CF594	CF647	CF754
3-plex		x	x		x	
4-plex		x	x		x	x
5-plex	x	x	x		x	x
6-plex	x	x	x	x	x	x

- For less than six-plex, favour dyes with well-separated fluorescence spectra detailed in Table 1.
- When possible, select dyes with well-separated spectra for antibodies staining the same cell type (e.g. CD8-CF488 and CD3-CF647 as both antigens are present in lymphocytes).
- Autofluorescence is higher for lower wavelengths (430–488 nm). Combine CF430 dye with highly expressed proteins.
- Filter sets with narrow band-passes (like the ones used for red dyes CF555 and AF594) should be associated to highly expressed proteins.
- On the opposite, filter sets with large band-passes (usually for CF488, CF647 and CF754 dyes) are preferentially selected for weakly expressed proteins.
- Dyes with close spectra (such as CF555, AF594 and CF647) can spill over into each other, but this is limited when staining intensity (transposed into scanning exposure time) in these channels is similar.
- Attention should be paid to the camera's sensitivity to higher-wavelength emissions to ensure adequate signal detection. If it drops, CF754 dye should be reserved for highly expressed markers.

2.3.3 | Multiplex panel design – position test

Some antigens are better unmasked after several HIER cycles whether others are damaged by repeated heating. To determine the best combination for a specific panel, each primary antibody is tested after successive staining cycles. A slide template for a six-plex position test is included in Table 2.

A specific position panel works for a specific set of antibodies. If one of them changes, the position test must be repeated.

The antibody properties are also taken into consideration:

- Some antigens are destroyed by heating (e.g. neutrophil elastase). Antibodies specific for such antigens are thus automatically placed at the first position.

TABLE 2 Template of position test.

	Position 1	Position 2	Position 3	Position 4	Position 5	Position 6
Slide A	Ab1	Ab2	Ab3	Ab4	Ab5	Ab6
Slide B	Ab6	Ab1	Ab2	Ab3	Ab4	Ab5
Slide C	Ab5	Ab6	Ab1	Ab2	Ab3	Ab4
Slide D	Ab4	Ab5	Ab6	Ab1	Ab2	Ab3
Slide E	Ab3	Ab4	Ab5	Ab6	Ab1	Ab2
Slide F	Ab2	Ab3	Ab4	Ab5	Ab6	Ab1

- Some antibodies display very high affinity for their antigen and do not withdraw well. These are then preferentially placed at the last position. Alternatively, they can also be stripped by two successive HIER steps at different pH.
- When CF754-tyramide is at the last position, an additional HIER step before counterstaining is needed to avoid background.

2.4 | Slide scanning

2.4.1 | Bright-field slide scanning

Slides stained by chromogenic IHC were digitalised using an automated slide scanner (NanoZoomer 2.0-RS, Hamamatsu Photonics K.K., Hamamatsu City, Japan).

2.4.2 | Fluorescence slide scanning

Whole slide imaging of slides stained in fluorescence was performed with a Zeiss Axioscan.z1 slide scanner (Oberkochen, Germany) using a 20×/0.8 Plan-Apochromat objective. With the aim to combine seven colours in a single scan, the most adequate combinations of seven fluorescent dyes and filter sets (composed of excitation, dichroic and emission filters) were selected using the Searchlight tool from Semrock. In the calculator module, illumination source (LEDs from Zeiss Colibri7) and camera (Hamamatsu OrcaFlash4.0 v3) were kept constant while several combinations of dyes and filter sets were estimated for:

1. Quantity of light reaching the camera.

This prediction of fluorescence detection efficacy allows to anticipate adequate detection of each dye but also exposure time needed for efficient detection (and hence scan duration).

For each filter set, fluorescence intensity was calculated for AlexaFluor (AF) or cyanine-based fluorescent (CF) dyes anticipated to be compatible.

Arbitrary scores of fluorescence intensity were attributed:

$> 1 \times 10^6$ mW: very high detection
$0.5–1 \times 10^6$ mW: high detection
$0.05–0.499 \times 10^6$ mW: low detection
$< 0.05 \times 10^6$ mW: no detection

2. Proportion of cross detection of other dyes for each filter (nonspecific signal).

For each filter set, fluorescence intensity was also calculated for other dyes destined to be combined in 7 colours staining.

Cross detection was calculated as:

$$\frac{\text{Fluorescence intensity of 'non} - \text{compatible' dye}}{\text{Fluorescence intensity of 'compatible' dye}} \times 100$$

Arbitrary scores of cross-detection were attributed:

> 20%: very high cross-detection
5%–19%: high cross-detection
1%–4%: moderate cross-detection
<1%: no cross-detection

The configuration found to be optimal is detailed in Figure S3. Of note, the file size of the scans (.czi format) were usually lightweight (around 100 Mo to 1 Go).

2.5 | Application example: breast cancer

2.5.1 | Tissue samples

Nineteen patients, diagnosed with a ductal carcinoma in situ (DCIS) of the breast, were selected. The samples originated from Cliniques universitaires Saint-Luc (Brussel, Belgium) and AZ Groeninge (Kortrijk, Belgium), sampled from 2005 to 2024. All samples were fixed in 10% neutral-buffered formalin for 8 to 72 h and embedded in paraffin. The mIHF were performed using a Leica Bond RXm autostainer and were scanned with a Zeiss Axioscan.z1 slide scanner.

For each sample, we collected information on the date of tissue collection, the type of surgical procedure (resection, vacuum-assisted biopsies (VAB) and core needle biopsies (CNB)), and the amount of adipose tissue (classified in four categories of fat/stroma ratio as previously described[9]). These tissue characteristics could potentially influence the efficiency of the protocol.

Common technical artefacts were also documented for the two staining panels: presence of cold zones (i.e. zones without immunostaining), presence of heterogeneous immunoreactivity (i.e. zones with variable staining intensity), and presence of tissue detachment. The tissue detachment was evaluated as absent (0%), focal (1%–20%), intermediate (21%–50%), extensive (51%–80%), or complete (>80%). The cold zone and heterogeneous staining were assessed as present or absent.

2.6 | Reproducibility

To assess the robustness of the Flex-6 mIHF protocol, a quantification analysis was performed on QuPath, version 5.1.[10] The mean fluorescence intensity of each dye on the on-slide control tissues was quantified. This analysis was performed across the different slides for each panel and therefore investigated the intra-run and inter-run reproducibility. Two different regions of interest (ROI) were selected: the entire control tissue sections and a selected area of 2 mm^2. Data were exported in SPSS to build graphs (version 29.02.0; IBM, Armonk, NY, USA).

3 | RESULTS

3.1 | Application example: breast cancer

We previously studied a cohort of 274 patients with DCIS at the morphological level.[11] DCIS is a non-obligate precursor of invasive breast cancer. We now aim to investigate the protein expression in both the tumour cells and the microenvironment to identify prognostic markers for upstaging of biopsy-diagnosed DCIS towards invasive cancer in the subsequent resection specimen. Because of its high fat content, breast cancer tissue is prone to detachment, which represents a challenge for IHC protocols. To evaluate the feasibility of mIHF on breast tissue sections, 10 representative samples were selected. Three subclasses of markers were investigated to explore the limits of this mIHF protocol: proteins expressed in tumours cells, in the ECM, and in inflammatory cells.

3.2 | Immunohistochemistry of 12 proteins on tissue controls

First, each antibody was validated by chromogenic IHC on positive tissue controls. In this way, specificity and signal-to-noise ratio can be assessed without the bias of tissue autofluorescence.

Many proteins routinely used in diagnostic histopathology practice are described on the website of NordiQC.[8] Appendix contains many different cell types, including lymphocytes and epithelial cells, as well as extracellular matrix in the submucosa. Normal appendix was therefore used as tissue control for all proteins of interest, except for EGFR and cyclin-D1. Placenta was used as a second tissue control to validate EGFR staining. Tonsil is recommended for cyclin-D1, since this tissue allows evaluation of cyclin-D1 expression in supra-basal squamous cells (which is absent in appendix). Tonsil is also appropriate for CD8, since it contains cytotoxic T lymphocytes.[12,13] Expected expression patterns are mentioned in Table 3.

Only two different on-slide tissue controls can be added in addition to the sample tissue section because the place on the slide is limited.

Among the four selected tumour markers, the normal expression pattern of p53 is wild-type immunostaining, characterised by a mixture of negative nuclei, weakly and moderate positive nuclei, resulting in a heterogeneous pattern.[14,15] As represented in Figure 1A, p53 was correctly stained in appendix tissue. EGFR was detected, as expected, in trophoblast of the placenta with a moderate to strong intensity of staining illustrated in Figure 1C, as described by Kosovic.[16] Synaptophysin was intensely expressed in ganglion cells and axons of Auerbach's and Meissner's plexus throughout the digestive tract, including the appendix as shown in Figure 1E.[17,18] Cyclin-D1 showed moderate to strong nuclear immunoreactivity in squamous epithelial cells, lymphocytes and endothelial cells, and a weak cytoplasmic staining of germinal centre macrophages of tonsil. The mantle zone B cells and germinal centre B cells were negative as expected, illustrated in Figure 1G.[12]

Among the four proteins expressed in lymphocytes, CD20 showed a very strong membranous immunoreactivity in the mantle zone and germinal centres.[19] CD3 and CD8 displayed an immunostaining in the membrane of the interfollicular area with a moderate to strong intensity and a strong intensity respectively, as expected.[13,20] FoxP3 was detected in the nuclei of regulatory T lymphocytes scattered in the appendix.[21] These immunostainings are illustrated in Figure 1I, K, M and O, respectively.

The four proteins we aimed to visualise in the ECM are not mentioned on the NordiQC website and are

TABLE 3 Expression patterns and subcellular localisation of proteins of interest, including selected on-slide tissue controls.

Markers	Subcellular localisation	Positive control tissue	Tissue subregion expression
Tumour cells			
p53*	Nucleus	Appendix	At least 50% of germinal centre B cells should be weakly to moderately positive. Less than 10% of the mantle zone B cells. Dispersed epithelial cells in the basal parts of the crypts should be weakly to moderately positive. Luminal epithelial cells should be negative.
EGFR	Membrane	Placenta	Trophoblastic cells (syncytiotrophoblast cells and cytotrophoblast cells) should be moderately to strongly positive.
Synaptophysin*	Cytoplasm	Appendix	Axons and ganglion cells in the myenteric plexus of the appendix should be strongly positive. Endocrine cells of the mucosa and peripheral nerves situated in lamina propria mucosa should be at least weakly to moderately positive.
Cyclin-D1*	Nucleus	Tonsil	All supra basal squamous epithelial cells and dispersed lymphocytes and endothelial cells should be moderately to strongly positive. Germinal centre macrophages should be weak. Mantle zone B cells and germinal centre B cells should be negative.
Inflammatory cells			
CD20*	Membrane	Appendix	The mantle zone and germinal centres of B cells should be moderately to strongly positive. T cells, stromal and epithelial cells should be negative.
CD3*	Membrane	Appendix	Aggregated T cells in interfollicular areas and dispersed T cells in mantle zone and germinal centres should be moderately to strongly positive. B cells should be negative. No cytoplasmic staining of columnar epithelial cells and plasma cells should be present.
FOXP3	Nucleus	Appendix	Regulatory T cells should be moderately to strongly positive. B cells should be negative.
CD8*	Membrane	Tonsil	All suppressor/cytotoxic T cells should be strongly positive. B cells, stromal cells and squamous epithelial cells should be negative.
Extracellular matrix			
Decorin	Stromal tissue	Appendix	Stromal tissue of the submucosa and the serous should be moderately to strongly positive. Epithelial cells and lymphocytes should be negative.
Versican	Stromal tissue	Appendix	Stromal tissue of the submucosa and the serous should be weakly positive. Epithelial cells and lymphocytes should be negative.
Biglycan	Stromal tissue	Appendix	Stromal tissue of the submucosa should be moderately to strongly positive. Epithelial cells and lymphocytes should be negative.
Lumican	Stromal tissue	Appendix	Stromal tissue of the submucosa should be moderately to strongly positive. Epithelial cells and lymphocytes should be negative.

*Data from NordiQC.

less frequently described in the literature. Decorin and versican are proteoglycans found in the ECM of many different organs.[22,23] A weak immunoreactivity of decorin has been shown in the ECM of normal pancreas, and in ECM and stromal cells of normal breast.[24,25] In normal colorectal tissue, lumican has been described with a weak to moderate intensity in fibroblasts, neural cells and mucosal/submucosal stromal tissues,[26,27] but epithelial cells should be negative.[28] Biglycan is predominantly present in the extracellular matrix and fibroblasts of normal pancreas tissue.[29]

Based on these previous reports and on data available on the website of The Human Protein Atlas, we extrapolated these findings to appendix. The four ECM proteins showed an expected immunoreactivity pattern (Figure 1Q, S, U and W).

Each marker was then stained in fluorescence using TSA. A different fluorescent dye was attributed to each

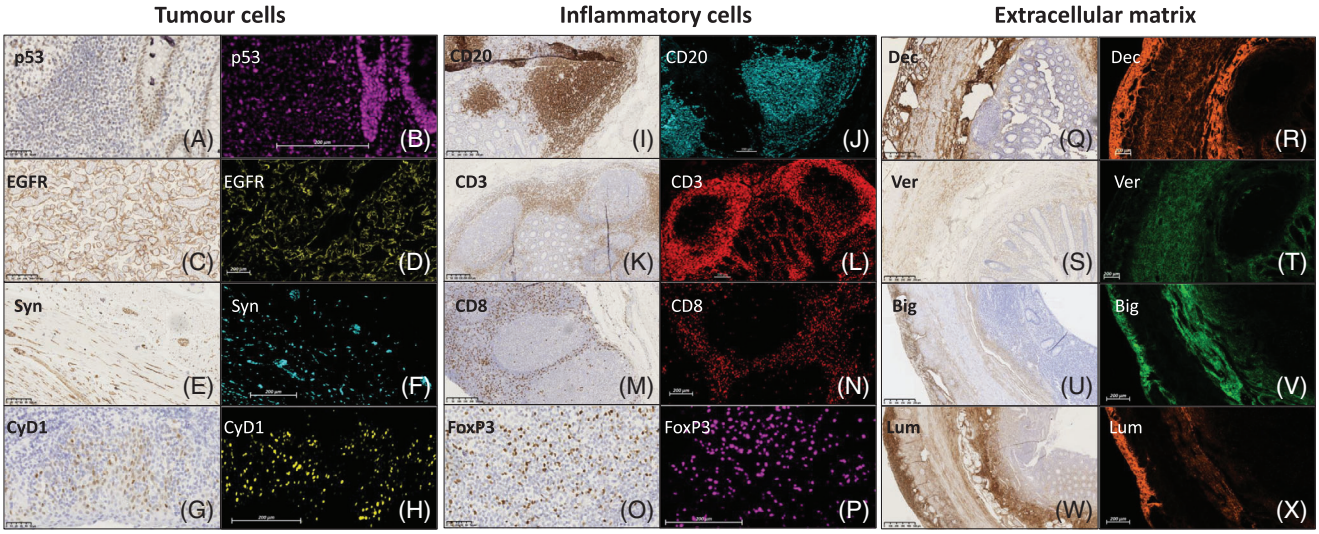

FIGURE 1 Validation of antibodies of interest. Each antibody was evaluated for its specificity and signal-to-noise ratio by IHC-DAB (left), and by IHF-TSA (right). (A, B) p53 on appendix, (C, D) EGFR on placenta, (E, F) synaptophysin on appendix, (G, H) cyclin-D1 on tonsil, (I, J) CD20 on appendix, (K, L) CD3 on appendix, (M, N) CD8 on tonsil, (O, P) FoxP3 on appendix, (Q, R) decorin on appendix, (S, T) versican on appendix, (U, V) biglycan on appendix, (W, X) lumican on appendix. Abbreviations: Syn: synaptophysin, CyD1: cyclin-D1, Dec: decorin, Vers: versican, Big: biglycan, Lum: lumican.

marker according to criteria explained in the Methods section. As depicted in Figure 1, staining analogous to DAB staining was observed and all markers were clearly distinct from the autofluorescence.

3.3 | Panels setup for multiplex immunohistofluorecence

The 12 markers were distributed in two six-plex panels, each of them comprising two tumour markers, two immune cell markers and two ECM markers. Panel 1 was composed of p53, EGFR, CD3, CD20, versican and decorin. Panel 2 consisted of cyclin-D1, synaptophysin, CD8, Foxp3, lumican and biglycan.

To determine the best sequence for a specific panel, each primary antibody was tested after successive staining cycles, as described in Table 2. The most adequate position for each antibody was determined according to different parameters: number of HIER, presence of HIER with a different pH before the target protein, staining intensity, signal-to-noise ratio, cross-detection in other channels and completeness of antibody stripping.

3.3.1 | Panel 1

The protocol of the position test applied to six consecutive slides of Panel 1 is schematised in Figure S4. Representative images of each marker at each position are displayed in Figure 2.

Staining intensity and specificity of EGFR and CD20 were not influenced by HIER cycles with a good signal-to-noise ratio from position 1 to 6 for both markers. CD3 and versican staining were weaker in position 1 and were either stable (versican) or more intense (CD3) after several HIER steps. Decorin showed a more homogeneous staining from position 4 to 6 and more specifically after two HIER at pH9. Finally, p53 showed a good signal-to-noise ratio for all positions with increasing intensity after several HIER cycles. However, from position 3 to 6, we observed a nonspecific staining, either due to cross detection of incompletely stripped CD20-CF430 or resulting from HIER at pH6 before incubation with the primary antibody for p53. These observations indicated that p53 should be placed either at position 1 or after other markers requiring HIER at pH9 (in this panel, EGFR only).

Taking all these observations into account, this led us to select the following staining sequence: EGFR/CF555 – p53/CF754 – versican/CF488 – CD3/AF594 – CD20/CF430 – decorin/CF647 (detailed conditions in Table 4, and references in Table S1).

3.3.2 | Panel 2

A similar position test was performed for the second panel. Lumican staining did not require HIER, so it was placed in position 1. Only biglycan displayed a good signal-to-noise ratio at position 2. All other markers required at least two HIER steps to overcome autofluorescence with increasing intensity according to HIER numbers. Foxp3,

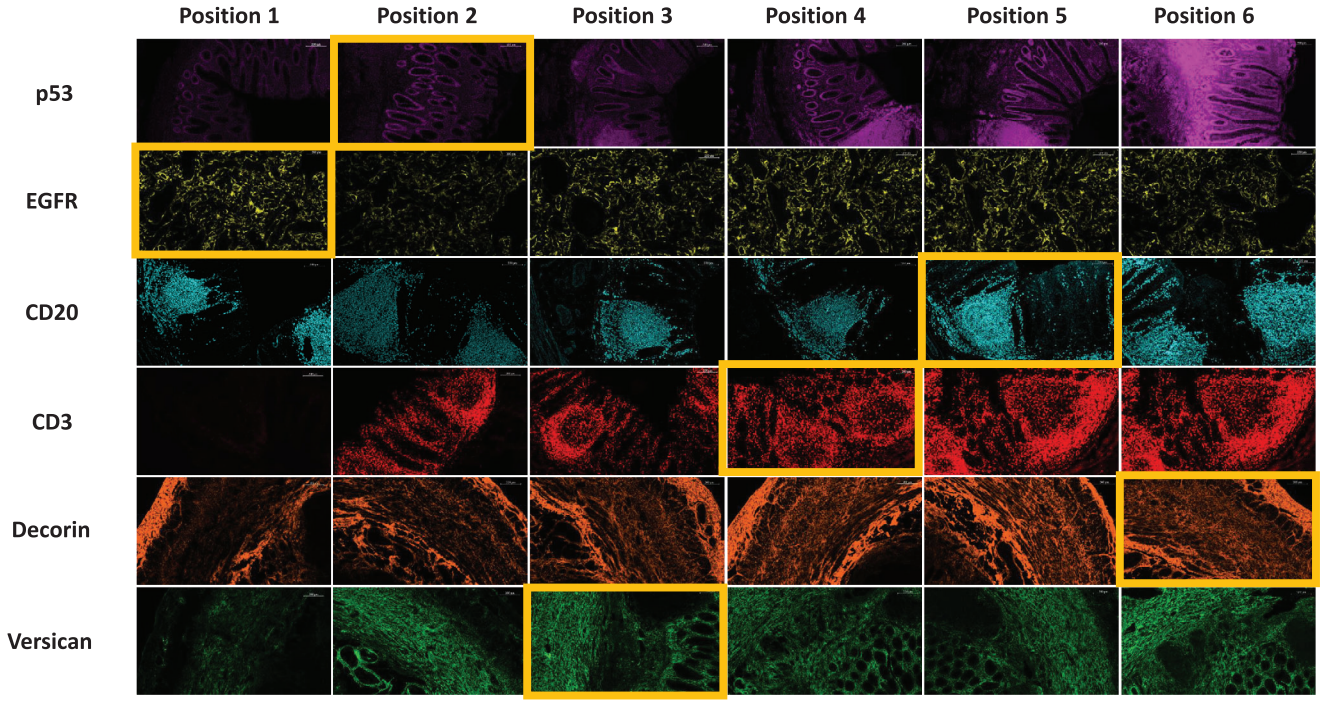

FIGURE 2 The position test of Panel 1 on tissue controls (appendix and placenta). Each marker is represented at each position. Acquisition and visualisation parameters were kept constant.

TABLE 4 Antibodies list for Panel 1.

Position	Antigen	Primary antibody Dilution	Primary antibody HIER method	Secondary antibody Polymer HRP	Tyramide Fluorochrome
1	EGFR	1/50	Tris-EDTA (pH9)	Anti-rabbit	CF555
2	p53	1/200	Tris-EDTA (pH9)	Anti-mouse	CF754
3	Versican	1/500	Citrate (pH6)	Anti-rabbit	CF488
4	CD3e	1/200	Citrate (pH6)	Anti-rabbit	AF594
5	CD20	1/200	Citrate (pH6)	Anti-mouse	CF430
6	Decorin	1/200	Citrate (pH6)	Anti-rabbit	CF647

synaptophysin and cyclin-D1 were satisfying at positions 3, 4 and 5, respectively. CD8 only reached a good intensity at position 6. The final sequence of this Panel 2 is illustrated in Figure S5 and consisted of lumican/CF647 – biglycan/CF488 – FoxP3/CF754 – synaptophysin/CF430 – cyclin-D1/CF555 – CD8/AF594. Experimental details of this panel are described in Table 5, and references in Table S1.

3.4 | Multiplex application on breast tissues: proof-of-principle

Subsequently, both six-plex protocols were tested on 10 breast tissue sections with DCIS to evaluate them on target tissue. Although the small number of samples did not allow to perform statistical analysis, we performed a qualitative evaluation of the different immunoreactivity patterns.

The staining quality was evaluated. Cyclin-D1 was overexpressed in three cases as illustrated in Figure 3A. When its expression was absent, the positive control was always present (Figure 3B). This observation is consistent with the literature describing an absence of cyclin-D1 staining in normal breast and an amplification of the *CCND1* gene in some tumours, resulting in nuclear overexpression (at least 10%) of the cyclin-D1 protein.[30,31] An intense homogenous staining of p53 was observed in two cases, and a weak to moderate heterogeneous immunoreactivity was observed for the others, illustrated in Figure 3C and D. Normal immunoreactivity for p53 is characterised by heterogeneous nuclear expression with varying intensity.

TABLE 5 Antibodies list for Panel 2.

Position	Antigen	Primary antibody Dilution	Primary antibody HIER method	Secondary antibody Polymer HRP	Tyramide Fluorochrome
1	Lumican	1/2500	/	Anti-rabbit	CF647
2	Biglycan	1/5000	Tris-EDTA (pH9)	Anti-rabbit	CF488
3	FOXP3	1/50	Citrate (pH6)	Anti-mouse	CF754
4	Synapto-physin	1/50	Citrate (pH6)	Anti-mouse	CF430
5	Cyclin-D1	1/100	Citrate (pH6)	Anti-rabbit	CF555
6	CD8	1/25	Citrate (pH6)	Anti-mouse	AF594

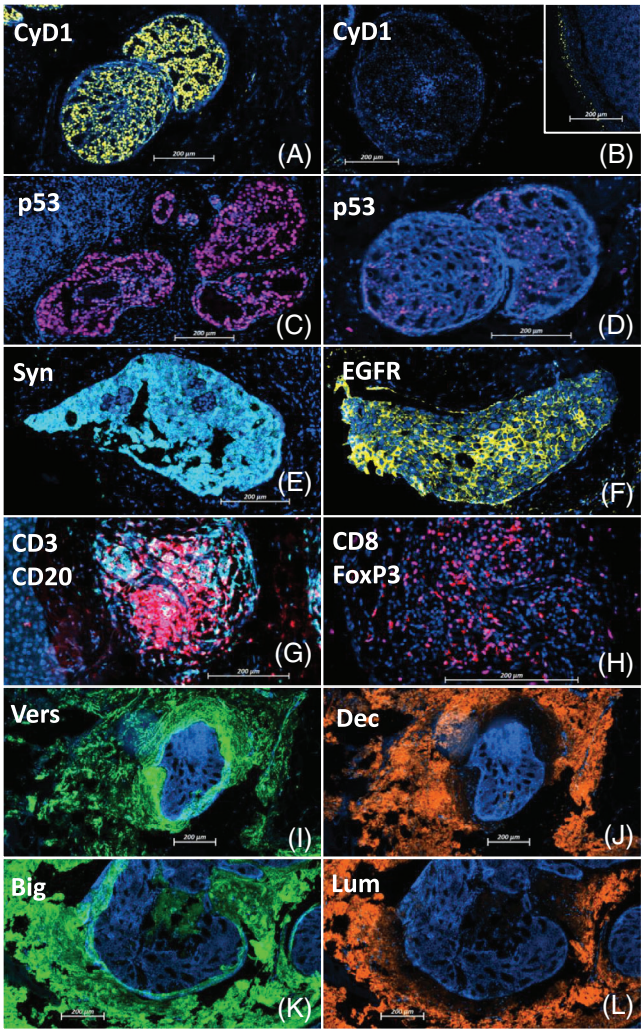

FIGURE 3 Illustration of the expression of each marker in breast cancer tissues. (A) Overexpression of cyclin-D1, (B) no expression of cyclin-D1 with a normal expression on tissue control, (C) wild-type p53, (D) overexpression of p53, (E) overexpression of synaptophysin, (F) overexpression of EGFR, (G) CD20 (blue) and CD3 (red), (H) CD8 (red) and FoxP3 (purple), (I) versican, (J) decorin, (K) biglycan, (L) lumican. Abbreviations: CyD1: cyclin-D1, Syn: synaptophysin, Vers: versican, Dec: decorin, Big: biglycan, Lum: lumican.

An abnormal immunoreactivity for p53 is defined either by overexpression (i.e. a diffuse moderate to strong uniform nuclear staining in at least 70% of tumour cells) or null pattern staining (i.e. total absence of nuclear staining) or diffuse cytoplasmic immunoreactivity without nuclear staining. These three 'mutation-type' staining patterns are suggestive of a *TP53* mutation.[32] Synaptophysin was overexpressed in one tissue (Figure 3E). Synaptophysin is not present in normal breast tissue but some breast cancers which present neuroendocrine differentiation, are characterised by a synaptophysin expression. The underlying mechanisms are unrelated to amplification or mutations.[33] We defined synaptophysin positivity as at least 50% tumour cells with strong cytoplasmic immunoreactivity.[34] Likewise, only one case presented an overexpression of EGFR (Figure 3F). *EGFR* gene amplification can result in EGFR protein overexpression in breast cancer, which is absent in normal breast tissue. The positivity of EGFR is defined by at least 50% of strong membrane immunoreactivity.[35] Inflammatory cells were dense and clustered close to ducts in three cases, as illustrated in Figure 3G and H. Five cases presented few scattered cells around ducts. The last case presented a situation between both.

Versican presented an increased intensity around affected ducts in five cases, illustrated in Figure 3I. The others were similar to the normal stroma present in the same slide. Most of cases (8/9) showed a decreased periductal intensity of decorin around tumour cells (Figure 3J). Lumican looked like decorin with a decreased intensity in six cases illustrated in Figure 3K. Biglycan seemed to be not impacted by tumours cells. Most of cases (7/9) presented a biglycan expression around affected ducts similar to the normal stroma (Figure 3L). Decorin, lumican and biglycan have been described previously as moderately to abundantly expressed in the ECM and stomal fibroblasts in normal breast tissue,[25,26,36] whereas versican is hardly expressed in normal breast stroma.[23,37] Decorin and versican were already described in some DCIS tumours, showing a downregulation of decorin and a trend of upregulation of versican associated with the presence of myxoid stroma.[38–40] Versican was also already

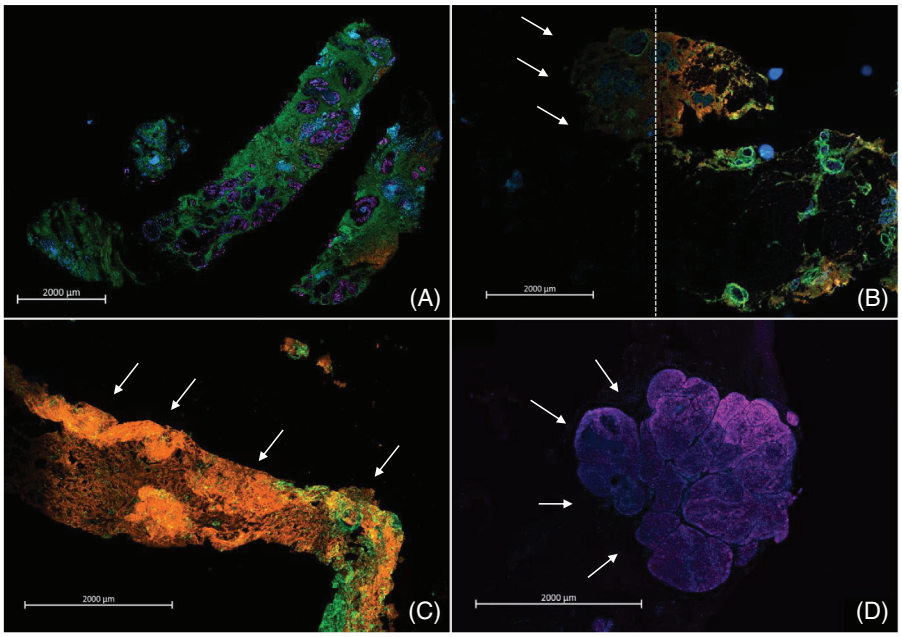

FIGURE 4 Artefacts on breast tissues after mHIF. (A) Tissue section without artefacts, (B) cold zone, (C) focal detachment, (D) heterogeneous staining of p53.

studied in breast cancer, and its increased immunoreactivity in the peritumoural stromal matrix was associated with the risk of recurrence.[23] Thiesen et al. found that biglycan was significantly lower in breast cancer tissue than in normal tissue.[36] A decreased stromal lumican expression is associated with a poor outcome in invasive breast cancer.[26]

The tissue sections used in this feasibility study comprised different sample types, including three surgical specimens, seven VAB and nine CNB, as detailed in Table 6. CNB are less invasive but give small specimens, whereas VAB result in larger samples, with a tissue surface similar to surgical specimens. Both are used for diagnosing breast lesions.[41] Almost 50% of the cohort presented ≥50% of fat content, characteristic of breast tissue.

Compared to a tissue section without artefacts (Figure 4A), three different technical issues were observed: cold zone (Figure 4B), tissue detachment (Figure 4C) and heterogeneous immunoreactivity (Figure 4D). For Panel 1, 63% of lesions did not present detachment (4/19–21%) or only a focal zone of detachment (8/19–42%). Five lesions (26%) presented an intermediate detachment, and two lesions (11%) were extensively detached, for which the fat content was >50%. A cold zone was observed in seven lesions (37%), among which six touched or extended beyond the edge of the coverslip. A heterogeneous staining for p53 was observed in two tissue samples (11%). For Panel 2, the frequency of detachment was similar to Panel 1 with 69% without detachment (2/19–11%) or presence of a focal detached zone (11/19–58%). Five lesions (26%) presented an intermediate detachment, and one tissue (5%) was considered as completely detached, for which the fat content was also >50%. A cold zone was observed in one sample (5%), which was a resection specimen. A heterogeneous staining for cyclin-D1 was observed in one sample (5%). These two last technical issues seemed to be independent from sample age, fat content and sample type. The tissue detachment seems to be affected by high fat content, but this technical issue appears to damage mainly the adipose tissue, thereby still allowing the tumour sample to be analysed.

3.5 | Reproducibility

The mean intensity of each dye was quantified, using two different annotations on the on-slide control tissues from different staining batches. Measured intensities were in the same range for each dye, regardless of the type of ROI, as shown in Figure S6. These data confirmed that Flex-6 mIHF yielded consistent results and allowed intra-run and inter-run reproducibility.

4 | DISCUSSION

Here, we demonstrated the feasibility of six-plex immunofluorescence staining on breast tissue samples using a non-commercial protocol, allowing co-localisation analyses in breast pathologies. Although it has never been

TABLE 6 Results on breast tissues.

Patient	Collection year	Fat/stroma ratio	Sample type	Panel	Detachment	Cold zone	Heterogeneous staining
1	2005	0%–24%	Resection	1	Intermediate	Present	Absent
				2	Focal	Absent	Absent
2	2014	75%–100%	VAB	1	Focal	Absent	Present for p53
				2	Focal	Absent	Absent
3	2015	50%–74%	CNB	1	Extensive	Present	Absent
				2	Complete	Absent	Absent
4	2015	25%–49%	CNB	1	Intermediate	Absent	Absent
				2	Intermediate	Absent	Absent
5	2017	50%–74%	VAB	1	Intermediate	Present	Absent
				2	Focal	Absent	Absent
6	2018	50%–74%	VAB	1	Focal	Absent	Absent
				2	Intermediate	Absent	Absent
7	2018	25%–49%	CNB	1	Absent	Absent	Absent
				2	Focal	Absent	Absent
8	2018	50%–74%	VAB	1	Focal	Present	Absent
				2	Focal	Absent	Absent
9	2018	25%–49%	Resection	1	Focal	Present	Absent
				2	Focal	Absent	Absent
10	2019	75%–100%	Resection	1	Absent	Present	Absent
				2	Absent	Present	Absent
11	2019	0%–24%	CNB	1	Intermediate	Present	Present for p53
				2	Intermediate	Absent	Absent
12	2021	50%–74%	VAB	1	Focal	Absent	Absent
				2	Focal	Absent	Absent
13	2022	25%–49%	VAB	1	Focal	Absent	Absent
				2	Focal	Absent	Absent
14	2022	0%–24%	CNB	1	Intermediate	Absent	Absent
				2	Intermediate	Absent	Absent
15	2022	50%–74%	VAB	1	Extensive	Absent	Absent
				2	Intermediate	Absent	Absent
16	2023	0%–24%	CNB	1	Focal	Absent	Absent
				2	Focal	Absent	Absent
17	2023	0%–24%	CNB	1	Focal	Absent	Absent
				2	Absent	Absent	Present for cyclin-D1
18	2023	0%–24%	CNB	1	Absent	Absent	Absent
				2	Focal	Absent	Absent
19	2024	0%–24%	CNB	1	Absent	Absent	Absent
				2	Focal	Absent	Absent

extensively detailed in prior publications, this protocol has previously been applied on several other tissues from different species. These include human and murine tumour samples, such as lung cancer, invasive breast cancer, colorectal carcinomas and melanoma,[42–46] non-tumoural tissues like lung, liver, pancreas and heart,[47–54] and also includes fragile tissues such as synovial biopsies and adipose tissue.[55–58] Breast tissue represents a specific challenge for multiplex staining, due to its frequent high fat content. In addition to the step-by-step protocol of multiplex immunofluorescence staining, this paper highlights the validation process leading to the combination of multiple markers in a single staining panel, for two different six-plex protocols. As shown in our application,

we encountered some artefacts. A non-exhaustive list of problems, their potential causes and our preventive recommendations were detailed in Table S3.

Commercial companies are often considered as the only option to supply staining kits and imaging equipment for detecting multiple proteins on a single tissue section. Among others, these include Akoya Phenocycler Fusion (formerly CODEX), Miltenyi MACSima, Lunaphore COMET, Ultivue InSituPlex, Bruker CellScape or Leica Cell Dive for direct or indirect IF; Akoya PhenoImager HT (formerly Phenoptics-Vectra Polaris), Cell Signaling SignalStar and Lunaphore SPYRE for signal amplification methods. These commercial solutions, even though providing most of the time high plexity, often come with a high cost, restriction to validated antibodies, time-consuming image processing and/or high footprint files. We highlight in Table S4 how the Flex-6 mIHF workflow positions among the major commercial technologies for aspects like principle of the technology, multiplexing depth, slide capacity per run, signal-to-noise ratio, infrastructure requirements, reagent dependence and image processing requirement.

To provide the scientific community with an open and cost-effective mIHF workflow, we developed a protocol using six non-OPAL tyramides matching carefully fine-tuned slide scanner configuration (LEDs and band-pass filtersets). This workflow does not require background subtraction nor spectral unmixing and allows the imaging of seven colours (six markers and a nuclear dye) with negligible cross-detection. Compared to commercial solutions, this protocol is flexible (compatible with any primary antibody), cheaper and faster (no image processing). Although image analysis was beyond the scope of this study, it is also worth to mention that this workflow generates lightweight image files (max 1.5 Gb per file vs. up to 50 Gb per file for commercial alternatives) that facilitate sharing and allow analysis on computers with a 'standard' configuration. A detailed report on digital analysis of the obtained images is beyond the scope of the present report. However, the generated images are fully compatible with commonly used computer-assisted image analysis software such as QuPath,[10] HALO® (Indicalab, New Mexico, USA), and Visiopharm Phenoplex™ (Visiopharm, Hoersholm, Denmark).

Regardless of the selected method, validation of primary antibodies is the cornerstone of immunostainings. The choice of appropriate tissue controls is crucial to assess staining specificity and intensity. An adequate positive control should contain at least one cell type with low to moderate expression of the protein of interest, to allow the evaluation of the sensitivity of the test. Normal tissues are preferred over pathological tissues since protein expression may vary among tumours, making them less reliable. The tissue section and its tissue controls should be placed at a distance from the slide borders to avoid cold zones, especially if using an autostainer.

In the present feasibility study using breast cancer samples, we used on-slide controls. This technique consists of mounting sections of the tissue control on the same slide as the target tissue and has two main advantages. Both tissues undergo the same treatment, confirming that the primary antibody is functional, even when it is not expressed in the target tissue.[59] It also serves as a control for slide-to-slide reproducibility. Including on-slide tissue controls in mIHF may be challenging due to limited space on a standard glass slide, allowing maximum two additional control tissues alongside the sample. Careful selection of tissue controls is thus essential. The appendix is a particularly useful option, as it contains a diverse range of cell types and structures. When combined with a second tissue chosen based on the target proteins, it can fulfil most control requirements.

Despite the above-mentioned advantages, the current Flex-6 mIHF protocol has some limitations. Firstly, only six antibodies can be stained on a single section. Indeed, TSA staining has restricted scalability due to the impossibility of detaching covalently bound fluorescent tyramides from the tissue section. This protocol is hence not intended to replace high-plex spatial technologies which enable profiling of dozens of markers simultaneously. This Flex-6 mIHF workflow rather provides an open alternative for targeted multiplex analyses. However, methods were recently described to bleach certain fluorophores (very stable over time), opening the way to iterative TSA staining. Among those, Iterative Bleaching Extends Multiplexity (IBEX, LiBH4-based and tissue-base cyclic immunofluorescence (t-CyCIF, NaOH/H2O2-based are promising).[6,60,61] Alternatively, a chromogenic IHC (multiplex or single stain) could also be performed on the same tissue section after the fluorescence multiplex IHC. Future research is needed to explore these possibilities. Secondly, caution is needed when targeting proteins that are expressed in a close vicinity (same cell type or ECM with intricate fibres) due to the risk of steric hindrance. For instance, we observed that increased stromal versican staining was accompanied by decreased stromal decorin staining. However, this is unlikely to be due to steric hindrance since we observed variable stromal lumican staining intensity in the presence of stable stromal biglycan immunoreactivity. Moreover, individual bright-field immunohistochemistry protocols previously showed a similar reverse expression pattern for stromal decorin and versican in DCIS.[40] Thirdly, in the situation of a six-plex where all markers present a weak immunoreactivity, fluorescence signal could be too low to overcome autofluorescence.

5 | CONCLUSION

In conclusion, the Flex-6 mIHF multiplex immunohistofluorescence is a co-staining method to investigate protein colocalisation in the tumour microenvironment. In comparison to most commercially available options, we proposed a more open, versatile and cost-effective workflow of low-plex mIHF. We demonstrated its feasibility on breast cancer tissues, independent from the age, size and fat content of the tissue samples. In the future, we aim to apply these two six-plex panels fine-tuned on the breast biopsy samples of a large-scale DCIS patient cohort. This flexible and affordable mIHF protocol offers the possibility to investigate protein colocalisation in (breast cancer) tissue samples of limited size. It will facilitate the understanding of the complex interplay between neoplastic cells and their microenvironment.

ACKNOWLEDGEMENTS

The authors are grateful to Ms. Dominique Dubois and Mr. Philippe Camby for their advising role in fine-tuning the individual immunohistochemistry protocols. Dr. Julia Riggi is supported by a research grant from the not-for-profit organisation Fund for Scientific Research-F.N.R.S. (Brussels, Belgium) as research fellow. Grant number: 40033175. Prof. Dr. Mieke Van Bockstal is supported by a research grant from the not-for-profit organisation Foundation Against Cancer (Brussels, Belgium). Grant number: 2025–048. The Axioscan has been funded by an equipment grant from Fund for Scientific Research-F.N.R.S. (Brussels, Belgium). Grant number: 35287957.

CONFLICT OF INTEREST STATEMENT

Open access publishing costs were paid by the firm Zeiss. The authors do not report any other conflict of interest regarding the present work.

ORCID

Julia A. M. Riggi https://orcid.org/0009-0005-8252-5111
Mieke R. Van Bockstal https://orcid.org/0000-0003-4498-928X
Caroline Bouzin https://orcid.org/0000-0003-0694-1947

REFERENCES

1. Tan, W. C. C., Nerurkar, S. N., Cai, H. Y., Ng, H. H. M., Wu, D., Wee, Y. T. F., Lim, J. C. T., Yeong, J., & Lim, T. K. H. (2020). Overview of multiplex immunohistochemistry/immunofluorescence techniques in the era of cancer immunotherapy. *Cancer Communications*, *40*(4), 135–153. https://doi.org/10.1002/cac2.12023
2. Viratham Pulsawatdi, A., Craig, S. G., Bingham, V., McCombe, K., Humphries, M. P., Senevirathne, S., Richman, S. D., Quirke, P., Campo, L., Domingo, E., Maughan, T. S., James, J. A., & Salto-Tellez, M. (2020). A robust multiplex immunofluorescence and digital pathology workflow for the characterisation of the tumour immune microenvironment. *Molecular Oncology*, *14*(10), 2384–2402. https://doi.org/10.1002/1878-0261.12764
3. Laberiano-Fernández, C., Hernández-Ruiz, S., Rojas, F., & Parra, E. R. (2021). Best practices for technical reproducibility assessment of multiplex immunofluorescence. *Frontiers in Molecular Biosciences*, *8*, 660202. https://doi.org/10.3389/fmolb.2021.660202
4. De Souza, N., Zhao, S., & Bodenmiller, B. (2024). Multiplex protein imaging in tumour biology. *Nature Reviews Cancer*, *24*(3), 171–191. https://doi.org/10.1038/s41568-023-00657-4
5. Najem, H., Pacheco, S., Turunen, J., Tripathi, S., Steffens, A., McCortney, K., Walshon, J., Chandler, J., Stupp, R., Lesniak, M. S., Horbinski, C. M., Winkowski, D., Kowal, J., Burks, J. K., & Heimberger, A. B. (2025). High dimensional proteomic multiplex imaging of the central nervous system using the COMET^{TM} system. *bioRxiv: The Preprint Server for Biology*, 2025.02.14.638299. https://doi.org/10.1101/2025.02.14.638299
6. Radtke, A. J., Chu, C. J., Yaniv, Z., Yao, L., Marr, J., Beuschel, R. T., Ichise, H., Gola, A., Kabat, J., Lowekamp, B., Speranza, E., Croteau, J., Thakur, N., Jonigk, D., Davis, J. L., Hernandez, J. M., & Germain, R. N. (2022). IBEX: An iterative immunolabeling and chemical bleaching method for high-content imaging of diverse tissues. *Nature Protocols*, *17*(2), 378–401. https://doi.org/10.1038/s41596-021-00644-9
7. Scheuermann, S., Kristmann, B., Engelmann, F., Nuernbergk, A., Scheuermann, D., Koloseus, M., Abed, T., Solass, W., & Seitz, C. M. (2024). Unveiling spatial complexity in solid tumor immune microenvironments through multiplexed imaging. *Frontiers in Immunology*, *15*, 1383932. https://doi.org/10.3389/fimmu.2024.1383932
8. NordiQC. (2025b). *NordiQC* [Lettre]. https://www.nordiqc.org/
9. Van Renterghem, S. M. J., Van Dorpe, J., Monstrey, S. J., Defreyne, J., Claes, K. E. Y., Praet, M., Verbeke, S. L. J., T'Sjoen, G. G. R., & Van Bockstal, M. R. (2018). Routine histopathological examination after female-to-male gender-confirming mastectomy. *The British Journal of Surgery*, *105*(7), 885–892. https://doi.org/10.1002/bjs.10794
10. Bankhead, P., Loughrey, M. B., Fernández, J. A., Dombrowski, Y., McArt, D. G., Dunne, P. D., McQuaid, S., Gray, R. T., Murray, L. J., Coleman, H. G., James, J. A., Salto-Tellez, M., & Hamilton, P. W. (2017). QuPath: Open source software for digital pathology image analysis. *Scientific Reports*, *7*(1), 16878. https://doi.org/10.1038/s41598-017-17204-5
11. Riggi, J., Galant, C., Benhaddi, N., Vernaeve, H., Vassilieff, M., Fellah, L., Leconte, I., Gerday, A., Coyette, M., Hammer, J., Berlière, M., & Van Bockstal, M. (2025). *Prognostic markers for upstaging of biopsy-diagnosed ductal carcinoma in situ of the breast*. Ghent Pathology.
12. Nielsen, S., Emanuelsen, L., & Røge, R. (2016). *Nordic Immunohistochemical Quality Control, CYD1 run 47*. https://www.nordiqc.org/downloads/assessments/82_41.pdf
13. Nielsen, S., Bzorek, M., & Emanuelsen, L. (2024a). *Nordic Immunohistochemical Quality Control, CD8 run 72*. https://www.nordiqc.org/downloads/assessments/189_22.pdf
14. Köbel, M., Ronnett, B. M., Singh, N., Soslow, R. A., Gilks, C. B., & McCluggage, W. G. (2019). Interpretation of P53 immunohistochemistry in endometrial carcinomas: Toward

increased reproducibility. *International Journal of Gynecological Pathology*, *38*(1), S123–S131. https://doi.org/10.1097/PGP.0000000000000488

15. Nielsen, S., Kristoffersen, H. L., & Emanuelsen, L. (2024). *Nordic Immunohistochemical Quality Control, p53 run 70*. https://www.nordiqc.org/downloads/assessments/187_60.pdf
16. Kosovic, I., Prusac, I. K., Berkovic, A., Marusic, J., Mimica, M., & Tomas, S. Z. (2017). Expression of EGF, EGFR, and proliferation in placentas from pregnancies complicated with preeclampsia. *Hypertension in Pregnancy*, *36*(1), 16–20. https://doi.org/10.1080/10641955.2016.1218502
17. Nielsen, S., Emanuelsen, L., & Røge, R. (2015). *Nordic Immunohistochemical Quality Control, SYP run 43*.
18. Nielsen, S., Emanuelsen, L., & Julio, T. (2025). *Nordic Immunohistochemical Quality Control, SYP run 73*.
19. Nielsen, S., Bzorek, M., & Emanuelsen, L. (2024b). *Nordic Immunohistochemical Quality Control, CD20 run 71*. https://www.nordiqc.org/downloads/assessments/188_27.pdf
20. Nielsen, S., Emanuelsen, L., Julio, T., & Kristoffersen, H. L. (2021). *Nordic Immunohistochemical Quality Control, CD3 run 63*. https://www.nordiqc.org/downloads/assessments/147_3.pdf
21. Hori, S., Nomura, T., & Sakaguchi, S. (2003). Control of regulatory T cell development by the transcription factor *Foxp3*. *Science*, *299*(5609), 1057–1061. https://doi.org/10.1126/science.1079490
22. Sawada, H., Shinomura, T., Kimata, K., Takeuchi, J., Tsuji, T., & Watanabe, H. (2002). Characterization of an anti-decorin monoclonal antibody, and its utility. *Journal of Biochemistry*, *132*(6), 997–1002. https://doi.org/10.1093/oxfordjournals.jbchem.a003315
23. Suwiwat, S., Ricciardelli, C., Tammi, R., Tammi, M., Auvinen, P., Kosma, V.-M., LeBaron, R. G., Raymond, W. A., Tilley, W. D., & Horsfall, D. J. (2004). Expression of extracellular matrix components versican, chondroitin sulfate, tenascin, and hyaluronan, and their association with disease outcome in node-negative breast cancer. *Clinical Cancer Research*, *10*(7), 2491–2498. https://doi.org/10.1158/1078-0432.CCR-03-0146
24. Köninger, J., Giese, N. A., Di Mola, F. F., Berberat, P., Giese, T., Esposito, I., Bachem, M. G., Büchler, M. W., & Friess, H. (2004). Overexpressed decorin in pancreatic cancer. *Clinical Cancer Research*, *10*(14), 4776–4783. https://doi.org/10.1158/1078-0432.CCR-1190-03
25. Oda, G., Sato, T., Ishikawa, T., Kawachi, H., Nakagawa, T., Kuwayama, T., Ishiguro, M., Iida, S., Uetake, H., & Sugihara, K. (2012). Significance of stromal decorin expression during the progression of breast cancer. *Oncology Reports*, *28*(6), 2003–2008. https://doi.org/10.3892/or.2012.2040
26. Brézillon, S., Pietraszek, K., Maquart, F.-X., & Wegrowski, Y. (2013). Lumican effects in the control of tumour progression and their links with metalloproteinases and integrins. *The FEBS Journal*, *280*(10), 2369–2381. https://doi.org/10.1111/febs.12210
27. Lu, Y. P., Ishiwata, T., Kawahara, K., Watanabe, M., Naito, Z., Moriyama, Y., Sugisaki, Y., & Asano, G. (2002). Expression of lumican in human colorectal cancer cells. *Pathology International*, *52*(8), 519–526. https://doi.org/10.1046/j.1440-1827.2002.01384.x
28. Seya, T., Tanaka, N., Shinji, S., Yokoi, K., Koizumi, M., Teranishi, N., Yamashita, K., Tajiri, T., Ishiwata, T., & Naito, Z. (2006). Lumican expression in advanced colorectal cancer with nodal metastasis correlates with poor prognosis. *Oncology Reports*, *16*(6), 1225–1230.
29. Weber, C. K., Sommer, G., Michl, P., Fensterer, H., Weimer, M., Gansauge, F., Leder, G., Adler, G., & Gress, T. M. (2001). Biglycan is overexpressed in pancreatic cancer and induces G1-arrest in pancreatic cancer cell lines. *Gastroenterology*, *121*(3), 657–667. https://doi.org/10.1053/gast.2001.27222
30. Frierson, H. F., Gaffey, M. J., Zukerberg, L. R., Arnold, A., & Williams, M. E. (1996). Immunohistochemical detection and gene amplification of cyclin D1 in mammary infiltrating ductal carcinoma. *Modern Pathology: An Official Journal of the United States and Canadian Academy of Pathology, Inc*, *9*(7), 725–730.
31. NordiQC. (2025a). *Cyclin D1* [Lettre]. https://www.nordiqc.org/epitope.php?id=41
32. Köbel, M., Hoang, L. N., Tessier-Cloutier, B., Meng, B., Soslow, R. A., Stewart, C. J. R., & Lee, C.-H. (2018). Undifferentiated endometrial carcinomas show frequent loss of core switch/sucrose nonfermentable complex proteins. *American Journal of Surgical Pathology*, *42*(1), 76–83. https://doi.org/10.1097/PAS.0000000000000941
33. Kawasaki, T., Mochizuki, K., Yamauchi, H., Inoue, S., Kondo, T., Oishi, N., Nakazawa, T., Yamane, T., Koshimizu, Y., Tsunoda, H., Yagata, H., Inoue, M., Inoue, A., Maruyama, T., Fujii, H., & Katoh, R. (2012). Neuroendocrine cells associated with neuroendocrine carcinoma of the breast: Nature and significance. *Journal of Clinical Pathology*, *65*(8), 699–703. https://doi.org/10.1136/jclinpath-2012-200765
34. Marchiò, C., Geyer, F. C., Ng, C. K., Piscuoglio, S., De Filippo, M. R., Cupo, M., Schultheis, A. M., Lim, R. S., Burke, K. A., Guerini-Rocco, E., Papotti, M., Norton, L., Sapino, A., Weigelt, B., & Reis-Filho, J. S. (2017). The genetic landscape of breast carcinomas with neuroendocrine differentiation: Genetics of neuroendocrine breast cancer. *The Journal of Pathology*, *241*(3), 405–419. https://doi.org/10.1002/path.4837
35. Viale, G., Rotmensz, N., Maisonneuve, P., Bottiglieri, L., Montagna, E., Luini, A., Veronesi, P., Intra, M., Torrisi, R., Cardillo, A., Campagnoli, E., Goldhirsch, A., & Colleoni, M. (2009). Invasive ductal carcinoma of the breast with the "triple-negative" phenotype: Prognostic implications of EGFR immunoreactivity. *Breast Cancer Research and Treatment*, *116*(2), 317–328. https://doi.org/10.1007/s10549-008-0206-z
36. Thiesen, A. P., Mielczarski, B., & Savaris, R. F. (2023). Deep learning neural network image analysis of immunohistochemical protein expression reveals a significantly reduced expression of biglycan in breast cancer. *PloS One*, *18*(3), e0282176. https://doi.org/10.1371/journal.pone.0282176
37. Skandalis, S. S., Labropoulou, V. T., Ravazoula, P., Likaki-Karatza, E., Dobra, K., Kalofonos, H. P., Karamanos, N. K., & Theocharis, A. D. (2011). Versican but not decorin accumulation is related to malignancy in mammographically detected high density and malignant-appearing microcalcifications in non-palpable breast carcinomas. *BMC Cancer*, *11*, 314. https://doi.org/10.1186/1471-2407-11-314
38. Doebar, S. C., De Monyé, C., Stoop, H., Rothbarth, J., Willemsen, S. P., & Van Deurzen, C. H. M. (2016). Ductal carcinoma in situ diagnosed by breast needle biopsy: Predictors of invasion in the excision specimen. *The Breast*, *27*, 15–21. https://doi.org/10.1016/j.breast.2016.02.014

39. Van Bockstal, M., Lambein, K., Gevaert, O., De Wever, O., Praet, M., Cocquyt, V., Van Den Broecke, R., Braems, G., Denys, H., & Libbrecht, L. (2013). Stromal architecture and periductal decorin are potential prognostic markers for ipsilateral locoregional recurrence in ductal carcinoma *in situ* of the breast. *Histopathology*, *63*(4), 520–533. https://doi.org/10.1111/his.12188
40. Van Bockstal, M., Lambein, K., Van Gele, M., De Vlieghere, E., Limame, R., Braems, G., Van den Broecke, R., Cocquyt, V., Denys, H., Bracke, M., Libbrecht, L., & De Wever, O. (2014). Differential regulation of extracellular matrix protein expression in carcinoma-associated fibroblasts by TGF-β1 regulates cancer cell spreading but not adhesion. *Oncoscience*, *1*(10), 634–648. https://doi.org/10.18632/oncoscience.87
41. Nakano, S., Imawari, Y., Mibu, A., Otsuka, M., & Oinuma, T. (2018). Differentiating vacuum-assisted breast biopsy from core needle biopsy: Is it necessary? *The British Journal of Radiology*, *91*(1092), 20180250. https://doi.org/10.1259/bjr.20180250
42. Aboubakar Nana, F., Hoton, D., Ambroise, J., Lecocq, M., Vanderputten, M., Sibille, Y., Vanaudenaerde, B., Pilette, C., Bouzin, C., & Ocak, S. (2019). Increased expression and activation of FAK in small-cell lung cancer compared to non-small-cell lung cancer. *Cancers*, *11*(10), 1526. https://doi.org/10.3390/cancers11101526
43. Derouane, F., Ambroise, J., Van Marcke, C., Van Bockstal, M., Berlière, M., Galant, C., Dano, H., Lougué, M., Benidovskaya, E., Jerusalem, G., Bours, V., Josse, C., Thiry, J., Daumerie, A., Bouzin, C., Corbet, C., & Duhoux, F. P. (2025). Response to neoadjuvant chemotherapy in early breast cancers is associated with epithelial–mesenchymal transition and tumor-infiltrating lymphocytes. *Molecular Oncology*, *19*(8), 2330–2347. https://doi.org/10.1002/1878-0261.13813
44. Farah, C., Neveu, M.-A., Bouzin, C., Knezevic, Z., Gallez, B., Leucci, E., Baurain, J.-F., Mignion, L., & Jordan, B. F. (2023). Hyperpolarized 13C-pyruvate to assess response to anti-PD1 immune checkpoint inhibition in YUMMER 1.7 melanoma xenografts. *International Journal of Molecular Sciences*, *24*(3), 2499. https://doi.org/10.3390/ijms24032499
45. Huyghe, N., Benidovskaya, E., Beyaert, S., Daumerie, A., Maestre Osorio, F., Aboubakar Nana, F., Bouzin, C., & Van Den Eynde, M. (2023). Multiplex immunofluorescence combined with spatial image analysis for the clinical and biological assessment of the tumor microenvironment. *Journal of Visualized Experiments*, (196), 65220. https://doi.org/10.3791/65220
46. Huyghe, N., Benidovskaya, E., Masoodi, T., Sinapi, I., De Cuyper, A., Vempalli, F., Beyaert, S., Bouzin, C., Osorio, F. M., Ferraro, L., Van Baren, N., Helaers, R., Goffette, P., Ghaye, B., Van Maanen, A., Castella, M.-L., Ceccarelli, M., Bedognetti, D., Galon, J., … Van Den Eynde, M. (2025). Impact of the tumor immune contexture in microsatellite-stable metastatic colorectal cancer treated with avelumab, cetuximab, and irinotecan. *Cell Reports Medicine*, *6*(7), 102201. https://doi.org/10.1016/j.xcrm.2025.102201
47. Ajith, A., Evraerts, J., Bouzin, C., Brusa, D., Merimi, M., Najar, M., Smets, F., Sokal, E., & Najimi, M. (2025). Progression to fibrosis and hepatocellular carcinoma in DEN CCl4 liver mice, is associated with macrophage and striking regulatory T cells infiltration. *Frontiers in Immunology*, *16*, 1601215. https://doi.org/10.3389/fimmu.2025.1601215
48. Buemi, A., Mourad, N. I., Bouzin, C., Devresse, A., Hoton, D., Daumerie, A., Zech, F., Darius, T., Kanaan, N., Gianello, P., & Mourad, M. (2024). Exploring preservation modalities in a split human pancreas model to investigate the effect on the islet isolation outcomes. *Transplantation Direct*, *10*(7), e1654. https://doi.org/10.1097/TXD.0000000000001654
49. Dechamps, M., De Poortere, J., Martin, M., Gatto, L., Daumerie, A., Bouzin, C., Octave, M., Ginion, A., Robaux, V., Pirotton, L., Bodart, J., Gerard, L., Montiel, V., Campion, A., Gruson, D., Van Dievoet, M.-A., Douxfils, J., Haguet, H., Morimont, L., … Beauloye, C. (2022). Inflammation-induced coagulopathy substantially differs between COVID-19 and septic shock: A prospective observational study. *Frontiers in Medicine*, *8*, 780750. https://doi.org/10.3389/fmed.2021.780750
50. Dufeys, C., Daskalopoulos, E.-P., Castanares-Zapatero, D., Conway, S. J., Ginion, A., Bouzin, C., Ambroise, J., Bearzatto, B., Gala, J.-L., Heymans, S., Papageorgiou, A.-P., Vinckier, S., Cumps, J., Balligand, J.-L., Vanhaverbeke, M., Sinnaeve, P., Janssens, S., Bertrand, L., Beauloye, C., & Horman, S. (2021). AMPKα1 deletion in myofibroblasts exacerbates post-myocardial infarction fibrosis by a connexin 43 mechanism. *Basic Research in Cardiology*, *116*(1), 10. https://doi.org/10.1007/s00395-021-00846-y
51. Gerard, L., Lecocq, M., Detry, B., Bouzin, C., Hoton, D., Pinto Pereira, J., Carlier, F., Plante-Bordeneuve, T., Gohy, S., Lacroix, V., Laterre, P.-F., & Pilette, C. (2024). Airway epithelium damage in acute respiratory distress syndrome. *Critical Care*, *28*(1), 350. https://doi.org/10.1186/s13054-024-05127-3
52. Jannone, G., Riani, E. B., De Magnée, C., Tambucci, R., Evraerts, J., Ravau, J., Baldin, P., Bouzin, C., Loriot, A., Gatto, L., Decottignies, A., Najimi, M., & Sokal, E. M. (2023). Senescence and senotherapies in biliary atresia and biliary cirrhosis. *Aging*, *15*(11), 4576–4599. https://doi.org/10.18632/aging.204700
53. Planté-Bordeneuve, T., Bertrand, Y., Lecocq, M., Hoton, D., Fillée, C., Lacroix, V., Rondelet, B., Wuyts, W., Bouzin, C., Pilette, C., & Froidure, A. (2024). The IgA-pIgR system is dysregulated in idiopathic pulmonary fibrosis. *American Journal of Respiratory and Critical Care Medicine*, *210*(6), 841–844. https://doi.org/10.1164/rccm.202401-0043LE
54. Santos-Ribeiro, D., Lecocq, M., De Beukelaer, M., Verleden, S., Bouzin, C., Ambroise, J., Dorfmuller, P., Yakoub, Y., Huaux, F., Quarck, R., Karmouty-Quintana, H., Ghigna, M.-R., Bignard, J., Nadaud, S., Soubrier, F., Horman, S., Perros, F., Godinas, L., & Pilette, C. (2023). Disruption of GCN2 pathway aggravates vascular and parenchymal remodeling during pulmonary fibrosis. *American Journal of Respiratory Cell and Molecular Biology*, *68*(3), 326–338. https://doi.org/10.1165/rcmb.2021-0541OC
55. Cascarano, L., Esfahani, H., Michel, P., Bouzin, C., Dessy, C., Balligand, J.-L., & Michel, L. Y. M. (2024). A matter of food and substrain: Obesogenic diets induce differential severity of cardiac remodeling in C57Bl/6J and C57Bl/6N substrains. *Physiological Genomics*, *56*(10), 649–660. https://doi.org/10.1152/physiolgenomics.00044.2024
56. Maistriaux, L., Foulon, V., Fievé, L., Xhema, D., Evrard, R., Manon, J., Coyette, M., Bouzin, C., Poumay, Y., Gianello, P., Behets, C., & Lengelé, B. (2024). Reconstruction of the human nipple–areolar complex: A tissue engineering approach. *Frontiers in Bioengineering and Biotechnology*, *11*, 1295075. https://doi.org/10.3389/fbioe.2023.1295075

57. Triaille, C., Tilman, G., Sokolova, T., Loriot, A., Marchandise, J., De Montjoye, S., Nzeusseu-Toukap, A., Méric De Bellefon, L., Bouzin, C., Galant, C., Durez, P., Lauwerys, B. R., & Limaye, N. (2023). Disease activity drives transcriptomic heterogeneity in early untreated rheumatoid synovitis. *Annals of the Rheumatic Diseases*, *82*(12), 1538–1546. https://doi.org/10.1136/ard-2023-224068
58. Triaille, C., Tilman, G., Baert, C. A., Sokolova, T., Loriot, A., Nzeusseu-Toukap, A., Meric De Bellefon, L., Galant, C., Boulanger, C., Fonseca, J. E., Bouzin, C., Durez, P., Lauwerys, B. R., & Limaye, N. (2024). Two broad categories overlapping with rheumatoid arthritis observed in synovial biopsies from patients with juvenile idiopathic arthritis. *Arthritis & Rheumatology*, *76*(9), 1439–1445. https://doi.org/10.1002/art.42922
59. Miller, R. T. (2019). Avoiding pitfalls in diagnostic immunohistochemistry–important technical aspects that every pathologist should know. *Seminars in Diagnostic Pathology*, *36*(5), 312–335. https://doi.org/10.1053/j.semdp.2019.05.002
60. Lin, J.-R., Izar, B., Wang, S., Yapp, C., Mei, S., Shah, P. M., Santagata, S., & Sorger, P. K. (2018). Highly multiplexed immunofluorescence imaging of human tissues and tumors using t-CyCIF and conventional optical microscopes. *eLife*, *7*, e31657. https://doi.org/10.7554/eLife.31657
61. Radtke, A. J., Kandov, E., Lowekamp, B., Speranza, E., Chu, C. J., Gola, A., Thakur, N., Shih, R., Yao, L., Yaniv, Z. R., Beuschel, R. T., Kabat, J., Croteau, J., Davis, J., Hernandez, J. M., & Germain, R. N. (2020). IBEX: A versatile multiplex optical imaging approach for deep phenotyping and spatial analysis of cells in complex tissues. *Proceedings of the National Academy of Sciences*, *117*(52), 33455–33465. https://doi.org/10.1073/pnas.2018488117

SUPPORTING INFORMATION

Additional supporting information can be found online in the Supporting Information section at the end of this article.

How to cite this article: Riggi, J. A. M., Daumerie, A., Benhaddi, N., Berlière, M., Galant, C., González-Antelo, A., Nana, F. A., Van Bockstal, M. R., & Bouzin, C. (2026). A detailed protocol for open and low-cost six-plex immunofluorescence (Flex-6 mIHF) with a proof-of-concept study on breast cancer tissue. *Journal of Microscopy*, 1–19. https://doi.org/10.1111/jmi.70068